Deformation analysis of ATHENA test filters made of plastic thin films supported by a mesh under differential static pressure

Nicola Montinaro
INAF - Osservatorio Astronomico di Palermo
Università degli Studi di Palermo
Palermo, Italy
orcid: 0000-0001-9607-3324
nicola.montinaro@inaf.it

Paolo Giglio
Università degli Studi di Palermo
Palermo, Italy

Elena Puccio
INAF - Osservatorio Astronomico di Palermo
Palermo, Italy

Fabio D'Anca
Istituto di BioFisica U.O.S. di Palermo – Consiglio Nazionale delle Ricerche
Palermo, Italy

Salvo Ferruggia Bonura
Università degli Studi di Palermo
Palermo, Italy

Marco Barbera
Università degli Studi di Palermo
Palermo, Italy

Ugo Lo Cicero
INAF - Osservatorio Astronomico di Palermo
Palermo, Italy

Daniele Gulli
INAF - Osservatorio Astronomico di Palermo
Palermo, Italy

***Abstract*— Within ESA Cosmic Vision 2015-2025 Science Program, ATHENA was selected to be a Large-class high energy astrophysics space mission. The observatory will be equipped with two interchangeable focal plane detectors named X-Ray Integral Field Unit (X-IFU) and Wide Field Imager (WFI). In order to optimally exploit the detector sensitivity, X-ray transparent filters are required. Such filters need to be extremely thin to maximize the X-ray transparency, that is, no more than a few tens of nm, still they must be able to sustain the severe stresses experienced during launch. Partially representative test filters were made with a thin polypropylene film, coated with Ti, and supported by a thin highly transparent mesh either in stainless steel or niobium. Differential static pressure experiments were carried out on two filter samples. In addition, the roles of the mesh on the mechanical deformation is studied, adopting a finite element model (FEM). The numerical analysis is compared with experimental results and found in good agreement. The FEM is a promising tool that allows to characterize materials and thicknesses in order to optimize the design.**

Keywords— Optical Profilometry, Stress Analysis, FEA, X-Ray, ATHENA, X-IFU.

I. Introduction

ATHENA (Advanced Telescope for High-Energy Astrophysics) was selected by ESA in the Cosmic Vision 2015-2025 Science Program as a Large-class astrophysics space mission, and it is scheduled to launch by 2030 [1]. The space observatory will be equipped with an X-ray telescope hosting two interchangeable focal plane detectors named X-ray Integral Field Unit (X-IFU) [2] and Wide Field Imager [3]. X-ray transparent filters are required for both detectors to work, optimally exploiting their sensitivity [4-6]. Specifically, the X-IFU operates at very low temperatures (<100 mK) within a cryostat. For this reason, thermal filters are required to reflect infrared (IR) light, to block molecular contamination and to dampen the load from radio frequency radiation, mainly coming from the telemetry. Filters need to be extremely thin to maximize X-ray transparency, just a few tens of nm, thus only light materials are employed: a polymer coated with a metal. However, the filters are required to survive severe launch conditions. Specifically, the X-IFU filters are currently planned to be launched in vacuum, meaning that they should be able to survive static pressure load, which may occur, for instance, during vacuum-venting procedures, and dynamic load which are mainly due to shock and vibrations.

Large size filters, made by a sub-micron thick polyimide film coated with aluminum, have already been largely used in recent space missions such as Chandra [7-8] and XMM-Newton [9]. Such filters have shown good reliability and long-term stability, having survived heavy launch loads, while being still in working order and showing no major signs of degradation [10]. Previous missions have thus indicated as a good solution a polyimide film coated in aluminum, to be used as a baseline for the X-IFU thermal filters. In addition, the large size of the filters together with the high load to be sustained, point towards adopting metallic meshes to act as a support for the polyimide film.

In this paper, to analyze the mechanical behavior of the metallic mesh when loaded with a differential static pressure, test films made in polypropylene were chosen for practical reasons. A set of experiments were carried out to acquire the displacement profile of a test filter as a function of the applied pressure. Furthermore, the experimental results were compared to the FEM numerical model ones to characterize the material and optimize filter design.

II. Experiments

A. Samples

The tested samples are partially representative of the filter that will operate inside the X-IFU cryostat at T = 2 K and T = 50 mK (see Fig. 1). Both filters are made of a polypropylene stretched foil (BASF Novolen 1302L), with thickness < 1 μm, coated with Ti and supported by a metallic mesh, mounted on a 2-part custom aluminum frame with 57 mm inner diameter. The two test samples which differ for the mesh material, respectively Nb and 304 SS, are

denominated: ATHENA-01-03-11 Rev A4-Exception Nb and ATHENA-01-03-11-A4 Rev. D57 S/N #2. In Table 1, specification of both test filters are reported.

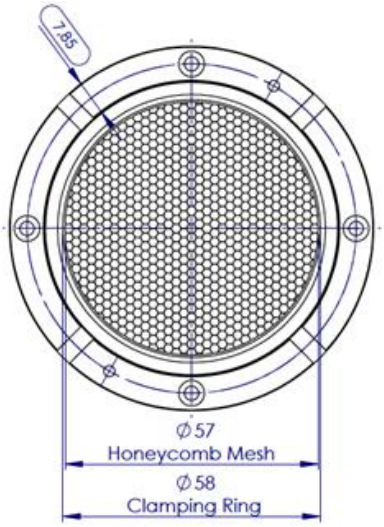

Fig. 1. X-IFU full size test filter representative of TF0 (operating at T = 50 mK) and TF2 (operating at T = 2K).

TABLE I. X-IFU TEST FILTER SPECIFICATIONS

	Sample 1	Sample 2
ID	***ATHENA-01-03-11 Rev A4-Exception Nb***	***ATHENA-01-03-11-A4 Rev. D57 S/N #2***
Film material	***Polypropylene stretched foil (BASF Novolen 1302L)***	
Film thickness	***~ 600 nm***	
Film Coating	***~ 40 nm thick Titanium coating***	
Mesh specs	***Honeycomb with pitch 2.0 mm and wire width 30µm Nominal transmission 97%***	
Mesh material	***Niobium Young Modulus 105 GPa Poisson coefficient 0.397***	***Stainless steel AISI 304 Young Modulus 210 GPa Poisson coefficient 0.3***
Mesh thickness	***50 µm***	***60 µm***
Filter frame	***Two parts style Aluminum alloy 6061 anticorodal***	

B. *Experimental setup*

The experimental setup comprises a custom micro-positioner, a filter holder, and an optical measuring system (see Figs. 2), with the aim of applying a static differential pressure and measuring sample deformation. The custom micro-positioner uses a pair of stepper motor micro-slides to allow control of the worktable speed and acceleration in the x and y axes. The filter holder is mounted directly on the worktable of the micro-positioner, which is controlled through a G-code user interface. The use of a sealing O-ring on the filter holder allows to apply a static pressure to the back part of the filter, by means of an air inlet hose connected to pressuring device. The pressuring device works with a Stevino column (1 mm reading accuracy equivalent to 0.1 mbar resolution) where a pre-determined amount of water is introduced plus a valve to expel air from the system. A schematic representation of the experimental setup is shown in Fig. 2a, while a picture of its realization is shown in Fig. 2b. The test filter deformation is measured by scanning its surface along a diameter. The pressure is gradually increased with steps of about 1 mbar and kept constant for all the duration of an acquisition.

The optical confocal sensor is a micro-epsilon® DT 2421/2422. The optical device comprises: the sensor along with its lens, the controller and the optical fiber. The measurement is based on the projection of a polychromatic light (white light) on the target surface. The sensor lenses are designed to use controlled chromatic aberration to focus each light wavelength at a specific distance. The sensor itself will then receive the light reflected from the target surface and transfer it to the controller. A spectral analysis follows and data stored in the controller are used to calculate distances. This system allows a very good resolution, thanks to the small beam spot diameter (see Table 2). However, measurement deviations may occur if the measured structure is of a similar size to the beam spot or if the maximum tilt angle is exceeded.

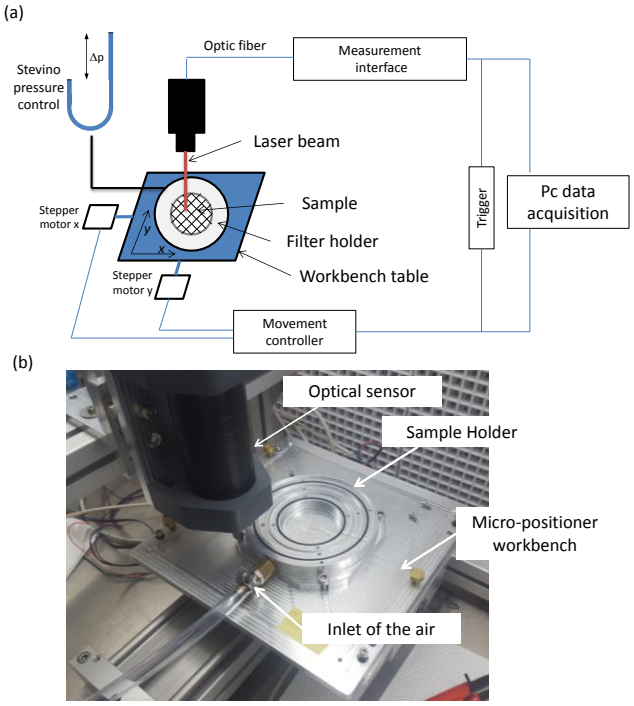

Fig. 2. In (a) schematic representation of the experimental setup; in (b) picture of the optical confocal acquiring system and of the micro-positioner.

TABLE II. OPTICAL MEASURING SYSTEM SPECIFICATIONS

Optical Sensor model 2405-10	
Measuring range	***10 mm***
Start of measuring range approx.	***50 mm***
Spot diameter	***16 µm***
Linearity (displacement measurement)	***≤± 2.5 µm***
Linearity (thickness measurement)	***≤± 5 µm***
Resolution	***60 nm***
Thickness measurement min target thickness	***0.5 mm***
Max. tilt	***±17 °***
Outer diameter sensor	***54 mm***

The scans of two test filters were performed under a static pressure going from 1 to 10 mbar. The scan speed used is a trade-off between duration and accuracy of the measure, a reasonable value was found to be 1 mm/s. In Fig. 3 a comparison between the profile of samples 1 and 2 at the

same pressure level (9 mbar) is shown, plotting the filter deflection (along the z-axis) as a function of the scanline distance (along the diameter).

The plot in Fig. 3a is affected by the presence of high spikes when the laser passes over the mesh bar edge. This is due to the marked difference in emissivity between the Ti coating of the film and the Nb mesh mar. The laser beam diameter (16 μm) is almost half the bar width, when the laser spot approaches the bar there is a multiple surface reflection, due to the very different emissivity, generating a spike. For this reason, an accurate measure of the mesh bar width and thickness can be made only for the stainless steel mesh, where the difference in emissivity with the Ti coating is less pronounced. More effort is needed to overcome this issue on the Nb mesh.

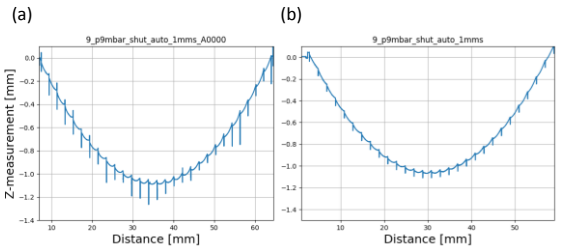

Fig. 3. Filter profile acquisition with a differential static pressure of 9 mbar for (a) Nb mesh and (b) AISI 304 mesh.

In Fig. 4 a plot compares the experimental maximum deflection, measured at the center of the filter, for both samples, as a function of the differential pressure.

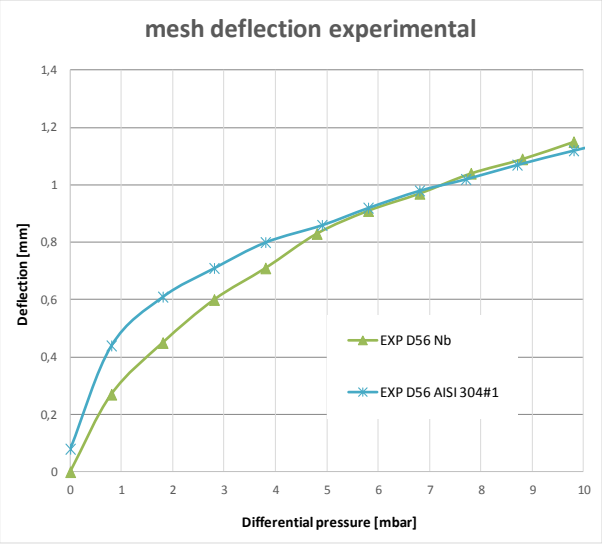

Fig. 4. Experimental deflection measured at the center of the filter at different differential pressures for the Nb and steel mesh.

Looking at Fig. 4 the unexpected result is that the Nb mesh deflection seems smaller than the steel mesh one, despite the Young modulus of Nb is expected to be almost half the steel one. However, from the graph it is also clear that for pressures above about 7 mbar, the two curves cross, indicating how at higher differential pressures the trend could reverse, in agreement with what one would expect. We have currently not applied a pressure larger than 10 mbar to prevent the risk of plastically deforming or damaging the filter.

A possible explanation for this uncharacteristic behavior at low pressures could be due to a different pre-stress in the films, glued to the mesh, during the manufacturing process, which could impact the overall structural stiffness.

III. Numerical Model

A static non-linear numerical model, simulating the deformation of the filters due to the differential pressure, was developed. Due to the thin geometry of the mesh, shell elements were adopted for discretization. Exploiting the structural symmetry, only a quarter of the filter was modeled, thus reducing computational cost. The perimeter of the mesh was simulated adopting an encastre to reproduce real conditions applied to the test filter (zero displacement and zero rotation). The pressure was applied gradually on the mesh bars, step by step, in order to avoid convergence issues. A preliminary convergence study was performed to fine tune the model. The discretization of the model was refined near the encastre due to stress intensification in these areas, as shown in Fig. 5. A total of 13200 S4R 4-node doubly curved thin shell elements were used to discretize a quarter of the mesh. Materials were modeled using a Young modulus (E) of 210 GPa and a Poisson coefficient (ν) of 0.3 for the AISI 304 mesh, a E of 105 GPa and a ν of 0.397 for the Nb mesh. In Fig. 5, the side and top view of the Nb mesh filter at 10 mbar of differential pressure, along with a legend of the von Mises stress, are shown. Because of the boundary conditions, where the mesh is attached to the frame, the deformation profile of the mesh external boundary starts flat (see encastre in Fig. 5), thus the stresses intensify in the mesh bar connected to the frame. As can be seen from the magnification on the right in Fig. 5b, the center of the filter is not affected by very high stresses. Still in the top view, the position of the maximum stress is located between a 30° and a 40° angle with the horizontal direction, and the magnification on the left shows how steep the stress gradient is in the mesh bars.

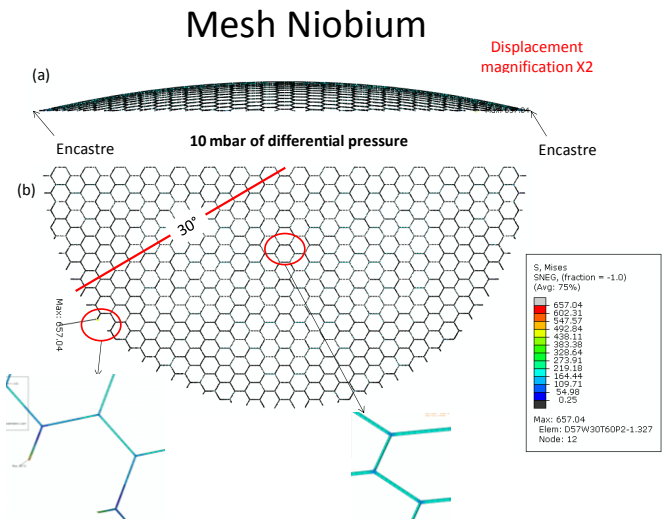

Fig. 5. Von Mises stress distribution over the Nb mesh with magnification of the boundary and center parts; in (a) side view, in (b) top view.

In Fig. 6, the side and top view of the steel mesh filter at 10 mbar of differential pressure, along with a legend of the von Mises stress, are shown. Similar considerations on the

stress distribution as what already detailed for the Nb mesh filter hold. The only differences regard the augmented von Mises stress level reached by the steel mesh and the subsequent smaller deflection, due to the enhanced stiffness of the material.

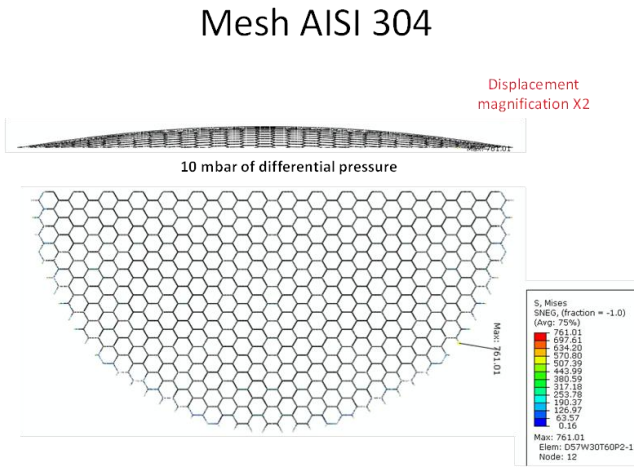

Fig. 6. Von Mises stress distribution over the AISI 304 mesh; in (a) side view, in (b) top view.

In Fig. 7, a plot to compare the modeled and experimental curves for both Nb and steel mesh is reported. As expected, the simulation indicates that the steel mesh exhibits a stiffer behavior than the Nb one. The best fit looks good for the steel mesh, with just a slight difference from the experimental data. For what concerns Nb, the difference is more marked, since the FEM analysis was run on the mesh alone and cannot take into account any pre-stress on the film, which, from the experimental data, could very well be present in this case.

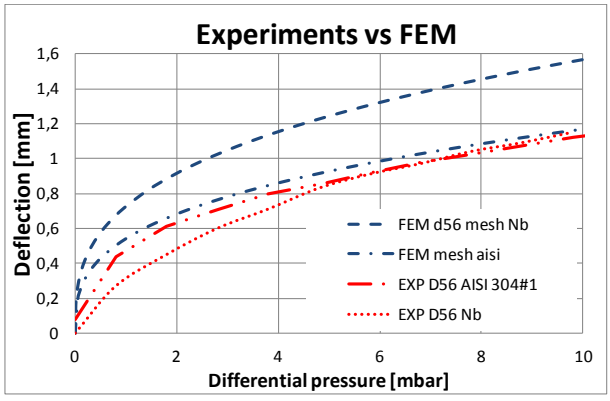

Fig. 7. Comparison between experimental and numerical results for the mximum deflection of both the Nb and steel mesh as a function of the differential pressure.

IV. Conclusions

The focal plane detector named X-Ray Integral Field Unit (X-IFU) to be equipped on the space observatory ATHENA needs specific filters able to maximize X-ray transparency. Filters need be extremely thin (just a few tens of nm) and still be able to sustain the severe stresses experienced during launch, plus they must survive any static pressure load which may occur during vacuum-venting procedures.

In this paper, the mechanical behavior of pre-assessment filters, made of a polypropylene film coated in Ti and supported by a metallic mesh, was tested by loading them with a differential static pressure. A set of experiments were carried out, by measuring the filter deflection as a function of the applied differential pressure with an optical confocal sensor.

Separately, the role of the Nb or steel mesh on the mechanical deformation was studied, adopting a finite element model (FEM). The numerical analysis results were then compared with the experimental ones and found in good agreement for the steel mesh, further raising interesting questions over potential pre-stress of the film supported by the Nb mesh. Future numerical analysis should be performed over the global system mesh plus film, under varying conditions.

Acknowledgments

The research leading to these results received funding from ASI (Italian Space Agency) under the contract n. 2015-046-R.0, from the European Union's Horizon 2020 Program under the AHEAD project (grant agreement n. 654215), and from ESA (European Space Agency) under the contract n. 4000120250/17/NL/BJ.

References

[1] X. Barcons, et al., "Athena: the X-ray observatory to study the hot and energetic Universe", Journal of Physics Conference Series, Volume 610, Issue 1, (2015). doi:10.1088/1742-6596/610/1/012008.

[2] D. Barret, et al., "The ATHENA X-ray Integral Field Unit (X-IFU)", Proc. SPIE 9905, 99052F-1, (2016). doi:10.1117/12.223243.

[3] N. Meidinger, et al., "The Wide Field Imager instrument for Athena", Proc. SPIE 10397, 103970V, (2017). doi:10.1117/12.2271844.

[4] M. Barbera, et al., "ATHENA X-IFU thermal filters development status toward the end of the instrument phase-A", (2018) Proc. SPIE, 10699, 106991R.

[5] M. Barbera, et al., "Thermal Filters for the ATHENA X-IFU: Ongoing Activities Toward the Conceptual Design", (2016) Journal of Low Temperature Physics, 184 (3-4), pp. 706-711.

[6] M. Barbera, et al., ATHENA WFI optical blocking filters development status toward the end of the instrument phase-A", (2018) Proc. SPIE, 10699, 106991E.

[7] M. Barbera, et al., "Development of the UV/ion shields for the Advanced X-ray Astrophysics Facility high-resolution camera (AXAF HRC)", Proc. SPIE 2280, 214-228 (1994). doi: 10.1117/12.186815.

[8] R. Meehan, et al., "Calibration of the UV/ion shields for the AXAF High-Resolution Camera", Proc. SPIE 3114, 74-100 (1997). doi: 10.1117/12.283790.

[9] G. E.Villa, et al., "The optical/UV filters for the EPIC experiment", IEEE Trans. on Nuclear Science, 45, 921-926 (1998).

[10] M. Barbera, et al., "The thin and medium filters of the EPIC camera on-board XMM-Newton: measured performance after more than 15 years of operation",(2016) Experimental Astronomy, 42 (2), pp. 179-197.